

Fluorination of Graphene Enhances Friction Due to Increased Corrugation

Qunyang Li,^{†,⊥,∇} Xin-Z. Liu,^{†,∇} Sang-Pil Kim,^{‡,#} Vivek B. Shenoy,[§] Paul E. Sheehan,^{||} Jeremy T. Robinson,^{||} and Robert W. Carpick^{*,†}

[†]Department of Mechanical Engineering and Applied Mechanics, University of Pennsylvania, 220 S. 33rd Street, Philadelphia, Pennsylvania 19104, United States

[‡]School of Engineering, Brown University, 184 Hope Street, Providence, Rhode Island 02912, United States

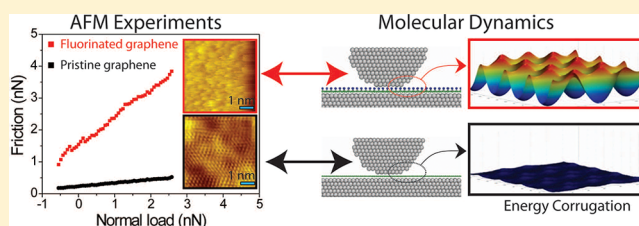
[§]Department of Materials Science and Engineering, University of Pennsylvania, 3231 Walnut Street, Philadelphia, Pennsylvania 19104, United States

^{||}Naval Research Laboratory, Washington, DC 20375, United States

S Supporting Information

ABSTRACT: The addition of a single sheet of carbon atoms in the form of graphene can drastically alter friction between a nanoscale probe tip and a surface. Here, for the first time we show that friction can be altered over a wide range by fluorination. Specifically, the friction force between silicon atomic force microscopy tips and monolayer fluorinated graphene can range from 5–9 times higher than for graphene. While consistent with previous reports, the combined interpretation from our experiments and molecular dynamics simulations allows us to propose a novel mechanism: that the dramatic friction enhancement results from increased corrugation of the interfacial potential due to the strong local charge concentrated at fluorine sites, consistent with the Prandtl-Tomlinson model. The monotonic increase of friction with fluorination in experiments also demonstrates that friction force measurements provide a sensitive local probe of the degree of fluorination. Additionally, we found a transition from ordered to disordered atomic stick–slip upon fluorination, suggesting that fluorination proceeds in a spatially random manner.

KEYWORDS: Fluorinated graphene, functionalization, friction, atomic stick–slip friction, energy corrugation



Friction, the force resisting the relative motion of two bodies in contact, is often controlled by the atomic-scale details at the sliding interface. For example, nanoscale friction is substantially altered by controlling the molecular tilt of a lipid monolayer¹ or by varying the mass of the terminating atoms on a surface.² It was also shown that by adding a few atomic layers of graphene, friction between an atomic force microscope (AFM) tip and a silicon surface was drastically reduced to values that were thickness-dependent: friction decreased monotonically as the number of layers increased.^{3,4} This was found to be caused by thickness-dependent puckering of graphene around the tip.² More recently, friction and adhesion anomalies were reported for both graphite and graphene: a negative effective friction coefficient,⁵ sliding-history dependent adhesion,⁶ and significant friction hysteresis for loading versus unloading directions,⁷ which are related to the chemical and mechanical state of the surface and the sliding history. Tuning the atomic details of a surface has thus emerged as a promising way of controlling interfacial friction and adhesion, which inevitably requires a better understanding of the correlation between surface atomic structure and friction.

The functionalization of graphene has attracted much attention recently as a means to engineer its intrinsic properties,

especially for electronic applications.^{8–10} Besides changing the electronic band gap, functionalization also influences friction significantly. Previous AFM measurements revealed that fluorinated graphene (FG) has much higher nanoscale friction than pristine graphene.¹¹ This was attributed to a fluorination-induced increase in out-of-plane stiffness.¹² In another study, FG was locally heated with an AFM tip to form reduced FG channels. These channels exhibited both higher conductivity and lower friction after reduction.¹³ Beyond fluorination, hydrogenation and oxidation of graphene were also found to increase friction.^{14–16} This behavior, observed in a humid environment, was attributed to a change in surface hydrophilicity, although the local hydrophilicity for hydrogenated and oxidized graphene was not measured.¹⁴ Dong et al.¹⁵ observed in molecular dynamics (MD) simulations that friction increased more than 20-fold as graphene was progressively hydrogenated; further hydrogenation then led to a decrease. These results are consistent with the experiments of Ko et al.,¹⁷ showing that various functionalized graphene monolayers exhibited higher friction forces compared to pristine graphene. However, the

Received: June 10, 2014

Published: July 29, 2014

MD simulations were for a vacuum environment, while the experiments were performed in ambient conditions, so the behavior may be related to the influence of ambient species including water vapor.

Furthermore, FG is the fundamental layered unit of graphite fluoride, common solid lubricant;¹⁸ in its fully fluorinated state, FG has been considered as a 2D analogue of Teflon.⁹ The importance of fluorinated carbon systems, coupled with the ongoing interest in the strong dependence of friction on fluorination and other functionalization chemistries motivate a more systematic investigation to better understand the underlying friction mechanism(s) of FG.

Here, friction between AFM tips and graphene fluorinated to varying degrees was measured, verified with Raman spectroscopy, and further studied with MD simulations. Fluorinated graphene samples were prepared using the technique described by Robinson et al.¹⁰ The selective fluorination, shown in Figure 1a–c, allowed us to interrogate pristine graphene regions alongside fluorinated regions using friction force microscopy (FFM) (see Methods Section).

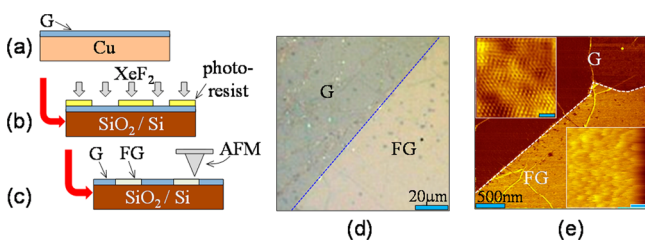


Figure 1. Preparation and characterization of patterned graphene fluoride. (a) CVD graphene growth on Cu foils; (b) graphene transfer and lithographic patterning on SiO₂/Si, followed by exposure to XeF₂ gas; (c) photoresist removal and AFM characterization at the boundary between G and FG. (d) Optical image at the boundary between G and FG after 10 min XeF₂ exposure; (e) AFM friction image at the boundary region in (d). Friction measured on FG (brighter region) is approximately 7 times of that on G (darker region); insets show high-resolution AFM images measured in the corresponding regions (see Supporting Information for more details). Inset scale bars represent 1 nm for G region and 2 nm for FG region.

Figure 1d shows a typical optical micrograph at a boundary between graphene (G) and FG of a patterned film on a SiO₂ (100 nm)/Si substrate. Optical contrast arises from the insulating nature of fluorinated graphene¹⁰ compared with pristine graphene. Within the fluorinated regions, we also observed small dark-colored islands, which are isolated graphene multilayers, as reported previously.¹⁰ AFM friction data collected across a graphene–FG boundary (Figure 1e) clearly shows that friction on FG is much higher than that on graphene (by a factor of ~ 7 for this sample; applied load was ~ 1.25 nN). In contrast to the regular atomic-lattice stick–slip friction observed in the graphene regions, only irregular discrete stick–slip events were observed in FG regions (Figure 1e, insets). This suggests that FG is not as ordered as pristine graphene.¹⁹ Furthermore, the well-ordered stick–slip in the graphene regions shows minimal contamination from processing.

To quantify frictional differences, we located the probe at the graphene–FG boundary and scanned repeatedly along a horizontal line crossing that boundary while ramping the normal load from high to low values. Friction versus normal load (data (Figure 2a) revealed nearly linear dependences of

friction on load, thus we used linear fits to determine the effective coefficients for FG and graphene, denoted μ_{FG} and μ_G , respectively. We find that μ_{FG} was ~ 6 times larger than μ_G for this sample.

We then examined samples exposed to systematically increased fluorination times, finding that friction on FG increased monotonically with fluorination time (Figure 2b). Raman spectra collected after the friction measurements (see Figure 2c) confirmed that the degree of fluorination increases with XeF₂ exposure time, as seen by the suppression of the 2D peak and the emergence and broadening of the D peak. X-ray photoelectron spectroscopy (XPS) on identically treated samples show an increase in the atomic F/C ratio of freshly prepared FG samples from 0.05 for a 1 min exposure to 0.7 at 20 min.²⁰ Thus, the friction enhancement depends directly and sensitively on the degree of fluorination of graphene. For samples exposed to XeF₂ for 150 s or longer, Figure 2b has a slope of $0.28 \pm 0.02 \text{ min}^{-1}$, indicating that each unit increase in friction ratio corresponds to 3.6 min of exposure or roughly a 13% increase in F/C ratio based on recent XPS studies.²⁰

Previously, increased capillary adhesion resulting from the increased hydrophilicity of graphene oxide compared to graphene was proposed to be the mechanism for enhanced friction observed on graphene oxide.¹⁴ Because the relative humidity was always kept very low in our AFM experiments ($< 2\%$), this mechanism is unlikely at play here. In addition, because FG is more hydrophobic than graphene,²¹ one would expect a reduction in capillarity and thus a reduction in frictional forces.

Recently, the theoretically calculated stiffness and the friction force were found to increase in tandem for hydrogenation, fluorination, and oxidation of graphene, respectively,^{11,12,22} suggesting a meaningful correlation. The authors hypothesized that because the increased flexural stiffness correlates with increased frequency of flexural phonons, higher friction may somehow result from more efficient energy dissipation. One physical feature not taken into account in this analysis is that in any elastic system, increased stiffness reduces contact area and, correspondingly, friction.²³ Furthermore, for pristine 2D materials including graphene, the increase in bending stiffness with increased number of layers was used to explain why friction decreases with increasing number of atomic layers.⁴ This mechanism occurs because for either suspended graphene or supported graphene on weakly adherent substrates thinner samples more easily pucker (deform out-of-plane) to adhere to the tip, increasing contact area and friction. As expected, the effect vanishes when out-of-plane deformation is suppressed in graphene supported on highly adhesive, atomically flat substrates.^{4,24} Because the out-of-plane flexural rigidity of FG is higher than that of graphene,^{9,11} a different mechanism is needed to explain the present results.

We carried out MD simulations of a nanoscale tip sliding on graphene sheets with various degree of fluorination, including pristine graphene, C₈F, and C₄F (see Methods Section).

Figure 3a shows the variation of friction with normal load for these simulations. Consistent with experiments, friction on all FG samples is much higher than on pristine graphene; the effective μ_{FG}/μ_G ratio ranges from 7.3:1 to 8.0:1. We did not observe any significant increase in puckering of FG compared to graphene (Supporting Information Figure S2). This excludes puckering⁴ as a mechanism for the observed friction enhancement.

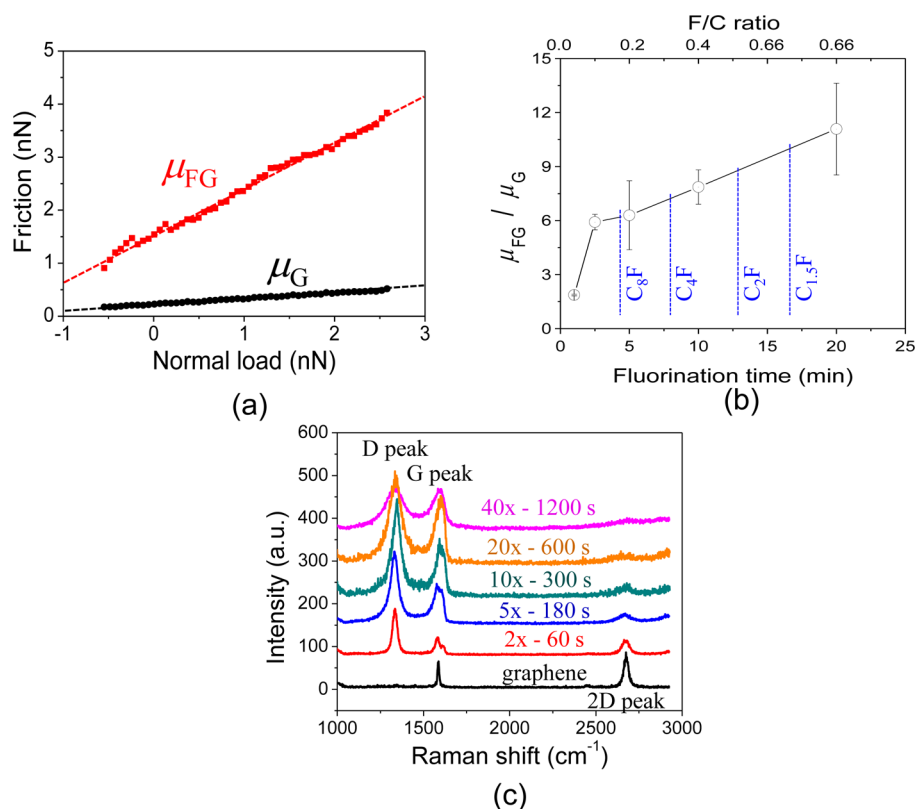


Figure 2. (a) Friction versus normal load data for pristine (red data points) and fluorinated graphene (600 s exposure, black data points) obtained by AFM scanning over a G/FG boundary. (b) Ratio of measured coefficient of friction (from linear fits to respective friction versus normal load plots) between fluorinated graphene and graphene, as a function of fluorination time. Labeled vertical lines indicate specific stoichiometries determined from XPS for corresponding fluorination times. (c) Raman spectra of graphene with various degrees of fluorination. As the exposure time increases, the intensity of 2D peak is suppressed and the D peak emerges indicating that graphene is becoming more and more fluorinated. Spectra were collected after the friction measurements (a few days after fabrication).

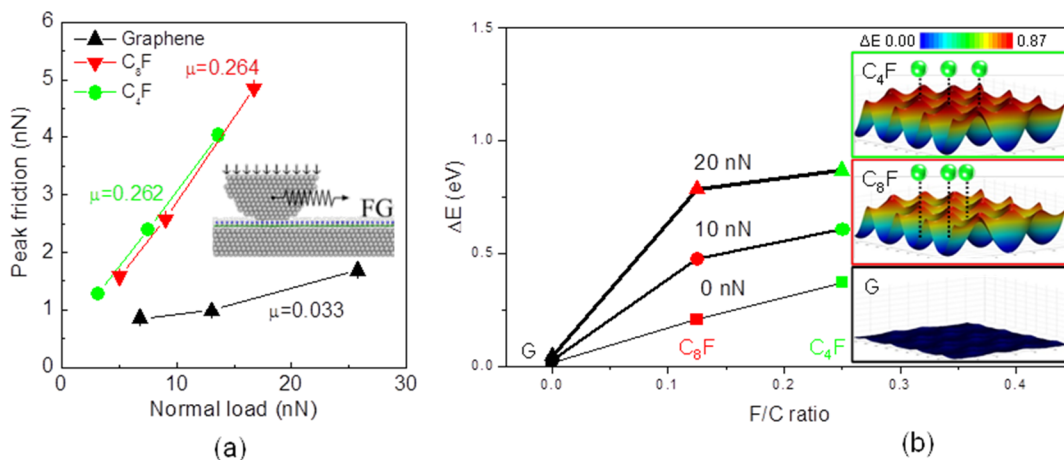


Figure 3. Results from MD simulations. (a) Friction as a function of normal load on pristine graphene, C_8F , and C_4F . Inset: snapshot of the simulated system showing the tip, sample, 2D film, and a schematic representing the lateral spring used to represent the cantilever. (b) Corrugation amplitude of the potential energy as a function of atomic content of fluorine on graphene from the simulations in (a). Insets: contour maps of the tip-sample potential energy for the same samples. Each map is shown for an area of $\sim 0.7 \times 1.0 \text{ nm}^2$. The color scale for all three maps ranges from 0 to 0.87 eV. Location of fluorine atoms are partially indicated by green spheres.

We then calculated the interaction energy between the tip and the sample as we varied the tip position. Three contour plots representing the spatial variation of tip-sample interaction energy for pristine graphene, C_8F , and C_4F are shown (Figure 3b, insets). We extracted the local amplitude of the potential energy variation (the energy corrugation) and

plotted it against the atomic fluorine content (Figure 3b), illustrating a strong dependence. For example, at 0 nN applied load pristine graphene exhibits a corrugation of only 12.9 meV, while the corrugation of C_8F is 206 meV, 15 times larger. Table 1 in Supporting Information lists the corrugation values, and

the ratios with respect to pristine graphene, for the three loads depicted in Figure 3.

The relationship between friction and corrugation has been extensively discussed.²⁵ The underlying physical behavior is explained by the Prandtl-Tomlinson (PT)²³ model that describes a spring-coupled entity sliding in a rigid one-dimensional sinusoidal potential at zero temperature. A transition from smooth, low friction sliding to unstable, higher friction occurs when the corrugation energy along the sliding direction E_0 exceeds $ka^2/2\pi^2$, where k is the lateral stiffness of the tip-sample contact (k accounts for elasticity of the cantilever and the contacting materials), and a is the lattice constant. In the stick-slip regime, the static friction F_f (the force at which slip occurs) is equal to $\pi E_0/a$. Indeed, for the MD results, $aF_f/\pi E_0$ is in the range of 2–5, consistent with the idea the PT model is a reasonable framework. We deem the MD simulations to be reliable, as they reproduced the experimental finding of greatly increased peak friction with increased fluorination. While care should be taken in comparing MD simulations with AFM experiments, Li et al.²⁶ recently showed very good agreement between energetic parameters, specifically the corrugation, extracted from MD simulations and well-matched experiments.

The enhanced corrugation is readily explained by the high electronegativity of the F atoms. The highly localized negative charge over F atoms as well as their protruding above the carbon basal plane leads to a strong local variation in the interfacial potential energy at fluorinated sites. Indeed, density functional theory calculations²⁷ have recognized that the electrostatic interaction originating from the polarized bonds between carbon and functional groups will dominate over the van der Waals interaction by altering the potential energy surface that in turn affects the friction behavior accordingly. Our results are also qualitatively consistent with the aforementioned MD simulations of hydrogenated graphene by Dong et al.,¹⁵ who predicted that partially hydrogenating the upper surface of graphene will increase friction, although no experimental data in vacuum have been reported to verify this result. They found that increased friction was unrelated to changes in adhesion or film elasticity, but rather was due to increased potential corrugation induced by the H atoms. Fessler et al. reported that hydrogenation increases friction for graphene and attributed this increase to hydrogenation-induced contamination. Cleaning the surface with the AFM tip reduces contamination and hence decreases the friction.¹⁶ Here, we extensively scanned the area of interest prior to friction measurements. We therefore do not expect this cleaning effect to affect the observed friction contrast.

The regular distribution of F atoms on graphene adopted in the simulations led to friction traces and energy corrugation maps that exhibit ordered patterns (see Supporting Information Figure SI-3 for details), in contrast to the disorder seen in experiments. Simulating model disordered FG samples gives qualitatively similar conclusions. Friction forces depended on the specific arrangement of the disordered F atoms, which is unknown experimentally, thus limiting the current simulations. (See Supporting Information Figure SI-4 for details.) It has been shown using generic atomistic simulations and a scaling analysis that for atomically flat surfaces disordered surfaces exhibit higher friction than ordered surfaces that are otherwise chemically identical.²⁸ Indeed, the results of Dong et al.¹⁵ show that disordered arrangements of H atoms can greatly increase friction on graphene. Therefore, despite differences between

simulations and experiments in the arrangement of F atoms, both are consistent with the hypothesis that fluorination greatly increases friction because of the corrugation induced by localized charge.

In conclusion, friction between silicon AFM tips and graphene is greatly enhanced by fluorination, consistent with previous studies. Friction increases monotonically with fluorination in experiments, demonstrating that AFM is a sensitive tool for characterizing the chemical state of fluorinated graphene. This effect is attributed to significantly altered energy landscape experienced by the tip due to fluorination. Static friction rises in proportion to this energy barrier in accordance with the Prandtl-Tomlinson model.

Methods. Graphene films were grown on copper foils using chemical vapor deposition,²⁹ then transferred to SiO₂/Si substrates.¹⁰ Transferred graphene samples were coated with a photoresist layer that was then patterned via optical lithography. Samples were then exposed to XeF₂ gas with various exposure time ranging from 60 to 1200 s at approximately 30 °C in a Xactix XeF₂ etching system at 1 Torr XeF₂ and 35 Torr N₂ carrier gas (in pulse mode). As the coated regions were protected by photoresist, only the uncoated regions were fluorinated. After XeF₂ exposure, the resist was subsequently removed in a short (~1 min.) acetone soak. After resist removal, pristine graphene regions are interrogated by friction force microscopy (AFM) side-by-side with fluorinated regions. For AFM measurements, an RHK UHV 350 AFM and an Asylum MFP-3D AFM were used, and the fluorinated graphene samples were continuously purged by clean, dry nitrogen (relative humidity measured to be <2%). The force sensors were silicon probes from Mikromasch (CSC37 type) with force constants calibrated by Sader's method³⁰ and a diamagnetic lateral force calibrator.³¹ Raman spectroscopy measurements were performed with an NTEGRA Spectra system (NT-MDT) with an excitation laser wavelength of 532 nm.

In the MD simulations performed in LAMMPS,³² a hemispherical Pt(111)-terminated asperity consisting of 1,626 atoms was sliding over graphene or FG supported by a stepped Pt(181) surface consisting of 5,280 atoms at 10 K of low temperature. The stepped Pt(181) surface qualitatively mimicked the atomic-level roughness of the SiO₂ substrate used in the experiments. The radius of the Pt tip was 2.3 nm, and the size of the Pt substrate was approximately 10 nm × 6 nm × 1.2 nm (length × width × height). Periodic boundary conditions were enforced at the edges along lateral directions. In our simulations, the interatomic interaction in fluorinated carbon systems was described by the reactive force-field (ReaxFF) potential³³ and the charge transfer effect was considered by the charge equilibration (QEq) method³⁴ at every MD step. The temperature of the system was controlled by the Berendsen thermostat, which rescales atom velocities every time step (each MD time step $\Delta t = 0.5$ fs). The normal load was controlled by adjusting the initial tip height from the film, and the topmost three layers of the tip atoms were allowed to move only along the sliding direction to prevent rotation of the tip during sliding. A virtual atom is introduced at 40 Å ahead of the tip and connected through a linear spring ($K = 80$ N/m) to mimic the lateral compliance of the AFM system. The speed of the virtual dragging atom was set to 2 m/s in all cases. The lateral force experienced by the spring was recorded at every 0.1 ps during the simulations. The peak values of lateral forces, that is, the static friction force, were used for comparison

because this depends directly on the energy corrugation according to the Prandtl-Tomlinson model.

■ ASSOCIATED CONTENT

Supporting Information

More experimental and simulation data are provided, including simulation on randomly distributed fluorinated graphene. This material is available free of charge via the Internet at <http://pubs.acs.org>.

■ AUTHOR INFORMATION

Corresponding Author

*E-mail: carpick@seas.upenn.edu.

Present Addresses

[†](Q.L.) AML and CNMM in School of Aerospace Engineering, Tsinghua University, Beijing 100084, China.

[#](S.P.K.) Samsung SDI R&D Center, 130 Samsung-ro, Suwon, Gyunggi 443–803, South Korea.

Author Contributions

[▽]Q.L. and X.Z.L. contributed equally.

Q.L. and X.Z.L. performed experiments, obtained the experimental data, and analyzed the data with input from all other authors. S.P.K. performed all simulations; V.B.S. supervised the simulation studies. J.T.R. prepared the G and FG samples. R.W.C. supervised the experimental work. The manuscript was written through contributions of all authors. All authors have given approval to the final version of the manuscript.

Notes

The authors declare no competing financial interest.

■ ACKNOWLEDGMENTS

This work was funded by the U.S. National Science Foundation under CMMI-1068741 and CMMI-1401164. Use of University of Pennsylvania Nano/Bio Interface Center instrumentation is acknowledged. Additionally, this research was partially supported by the Nano/Bio Interface Center through the National Science Foundation under NSEC DMR08-32802 and NSF Major Research Instrumentation Grant DMR-0923245 is acknowledged for the use of the NT-MDT Raman spectrometer. S.P.K. acknowledges the support of the Extreme Science and Engineering Discovery Environment (XSEDE), which is supported by National Science Foundation Grant DMR-090098 and MSS-130003 and also the support of Korea Institute of Machinery and Materials through KIMM-Brown International Cooperative Research Program. V.B.S. acknowledges the support from the NSF under Grant CMMI1308396. The work at the Naval Research Laboratory was funded through Base Programs via the Office of Naval Research.

■ REFERENCES

- (1) Liley, M.; Gourdon, D.; Stamou, D.; Meseth, U.; Fischer, T. M.; Lutz, C.; Stahlberg, H.; Vogel, H.; Burnham, N. A.; Duschl, C. Friction anisotropy and asymmetry of a compliant monolayer induced by a small molecular tilt. *Science* **1998**, *280*, 273–275.
- (2) Cannara, R. J.; Brukman, M. J.; Cimat, K.; Sumant, A. V.; Baldelli, S.; Carpick, R. W. Nanoscale friction varied by isotopic shifting of surface vibrational frequencies. *Science* **2007**, *318*, 780–3.
- (3) Filleter, T.; McChesney, J. L.; Bostwick, A.; Rotenberg, E.; Emtsev, K. V.; Seyller, T.; Horn, K.; Bennewitz, R. Friction and Dissipation in Epitaxial Graphene Films. *Phys. Rev. Lett.* **2009**, *102*, 086102.

- (4) Lee, C.; Li, Q. Y.; Kalb, W.; Liu, X. Z.; Berger, H.; Carpick, R. W.; Hone, J. Frictional Characteristics of Atomically Thin Sheets. *Science* **2010**, *328*, 76–80.

- (5) Deng, Z.; Smolyanitsky, A.; Li, Q. Y.; Feng, X. Q.; Cannara, R. J. Adhesion-dependent negative friction coefficient on chemically modified graphite at the nanoscale. *Nat. Mater.* **2012**, *11*, 1032–1037.

- (6) Liu, X.-Z.; Li, Q.; Egberts, P.; Carpick, R. W. Nanoscale adhesive properties of graphene: The effect of sliding history. *Adv. Mater. Interfaces* **2014**, *1*, 1–9.

- (7) Egberts, P.; Han, G. H.; Liu, X. Z.; Johnson, A. T. C.; Carpick, R. W. Frictional Behavior of Atomically Thin Sheets: Hexagonal-Shaped Graphene Islands Grown on Copper by Chemical Vapor Deposition. *ACS Nano* **2014**, *8* (5), 5010–5021.

- (8) Elias, D. C.; Nair, R. R.; Mohiuddin, T. M. G.; Morozov, S. V.; Blake, P.; Halsall, M. P.; Ferrari, A. C.; Boukhvalov, D. W.; Katsnelson, M. I.; Geim, A. K.; Novoselov, K. S. Control of Graphene's Properties by Reversible Hydrogenation: Evidence for Graphane. *Science* **2009**, *323*, 610–613.

- (9) Nair, R. R.; Ren, W. C.; Jalil, R.; Riaz, I.; Kravets, V. G.; Britnell, L.; Blake, P.; Schedin, F.; Mayorov, A. S.; Yuan, S. J.; Katsnelson, M. I.; Cheng, H. M.; Strupinski, W.; Bulusheva, L. G.; Okotrub, A. V.; Grigorieva, I. V.; Grigorenko, A. N.; Novoselov, K. S.; Geim, A. K. Fluorographene: A Two-Dimensional Counterpart of Teflon. *Small* **2010**, *6*, 2877–2884.

- (10) Robinson, J. T.; Burgess, J. S.; Junkermeier, C. E.; Badescu, S. C.; Reinecke, T. L.; Perkins, F. K.; Zalalutdniov, M. K.; Baldwin, J. W.; Culbertson, J. C.; Sheehan, P. E.; Snow, E. S. Properties of Fluorinated Graphene Films. *Nano Lett.* **2010**, *10*, 3001–3005.

- (11) Kwon, S.; Ko, J.-H.; Jeon, K.-J.; Kim, Y.-H.; Park, J. Y. Enhanced Nanoscale Friction on Fluorinated Graphene. *Nano Lett.* **2012**, *12* (12), 6043–6048.

- (12) Ko, J. H.; Kwon, S.; Byun, I. S.; Choi, J. S.; Park, B. H.; Kim, Y. H.; Park, J. Y. Nanotribological Properties of Fluorinated, Hydrogenated, and Oxidized Graphenes. *Tribol. Lett.* **2013**, *50*, 137–144.

- (13) Lee, W.-K.; Haydell, M.; Robinson, J. T.; Laracuente, A. R.; Cimpoiu, E.; King, W. P.; Sheehan, P. E. Nanoscale Reduction of Graphene Fluoride via Thermochemical Nanolithography. *ACS Nano* **2013**, *7* (7), 6219–6224.

- (14) Byun, I. S.; Yoon, D.; Choi, J. S.; Hwang, I.; Lee, D. H.; Lee, M. J.; Kawai, T.; Son, Y. W.; Jia, Q.; Cheong, H.; Park, B. H. Nanoscale Lithography on Mono layer Graphene Using Hydrogenation and Oxidation. *ACS Nano* **2011**, *5*, 6417–6424.

- (15) Dong, Y. L.; Wu, X. W.; Martini, A. Atomic roughness enhanced friction on hydrogenated graphene. *Nanotechnology* **2013**, *24*, 6.

- (16) Fessler, G.; Eren, B.; Gysin, U.; Glatzel, T.; Meyer, E. Friction force microscopy studies on SiO₂ supported pristine and hydrogenated graphene. *Appl. Phys. Lett.* **2014**, *104*, 041910.

- (17) Ko, J.-H.; Kwon, S.; Byun, I.-S.; Choi, J. S.; Park, B. H.; Kim, Y.-H.; Park, J. Y. Nanotribological Properties of Fluorinated, Hydrogenated, and Oxidized Graphenes. *Tribol. Lett.* **2013**, *50* (2), 137–144.

- (18) Watanabe, N.; Nakajima, T.; Touhara, H. *Graphite Fluorides*; Elsevier: Amsterdam, 1988.

- (19) Jeon, K.-J.; Lee, Z.; Pollak, E.; Moreschini, L.; Bostwick, A.; Park, C.-M.; Mendelsberg, R.; Radmilovic, V.; Kostecki, R.; Richardson, T. J.; Rotenberg, E. Fluorographene: A Wide Bandgap Semiconductor with Ultraviolet Luminescence. *ACS Nano* **2011**, *5*, 1042–1046.

- (20) Stine, R.; Lee, W.-K.; Whitener, K. E., Jr.; Robinson, J. T.; Sheehan, P. E. Chemical stability of graphene fluoride produced by exposure to XeF₂. *Nano Lett.* **2013**, *13*, 4311–6.

- (21) Hernández, S. C.; Bennett, C. J. C.; Junkermeier, C. E.; Tsoi, S. D.; Bezare, F. J.; Stine, R.; Robinson, J. T.; Lock, E. H.; Boris, D. R.; Pate, B. D.; Caldwell, J. D.; Reinecke, T. L.; Sheehan, P. E.; Walton, S. G. Chemical Gradients on Graphene To Drive Droplet Motion. *ACS Nano* **2013**, *7*, 4746–4755.

- (22) Lee, W. K.; Haydell, M.; Robinson, J. T.; Laracuente, A. R.; Cimpoiu, E.; King, W. P.; Sheehan, P. E. Nanoscale Reduction of Graphene Fluoride via Thermochemical Nanolithography. *ACS Nano* **2013**, *7*, 6219–6224.

(23) Mate, C. M. *Tribology on the Small Scale: A Bottom Up Approach to Friction, Lubrication, and Wear*; Oxford University Press: New York, 2008.

(24) Cho, D. H.; Wang, L.; Kim, J. S.; Lee, G. H.; Kim, E. S.; Lee, S.; Lee, S. Y.; Hone, J.; Lee, C. Effect of surface morphology on friction of graphene on various substrates. *Nanoscale* **2013**, *5*, 3063–9.

(25) Socoliuc, A.; Bennewitz, R.; Gnecco, E.; Meyer, E. Transition from stick-slip to continuous sliding in atomic friction: entering a new regime of ultralow friction. *Phys. Rev. Lett.* **2004**, *92*, 134301.

(26) Li, Q.; Dong, Y.; Perez, D.; Martini, A.; Carpick, R. W. Speed Dependence of Atomic Stick-Slip Friction in Optimally Matched Experiments and Molecular Dynamics Simulations. *Phys. Rev. Lett.* **2011**, *106*, 126101.

(27) Wang, L. F.; Ma, T. B.; Hu, Y. Z.; Wang, H.; Shao, T. M. Ab Initio Study of the Friction Mechanism of Fluorographene and Graphane. *J. Phys. Chem. C* **2013**, *117*, 12520–12525.

(28) Muser, M. H.; Wenning, L.; Robbins, M. O. Simple microscopic theory of Amontons's laws for static friction. *Phys. Rev. Lett.* **2001**, *86*, 1295–1298.

(29) Li, X.; Cai, W.; An, J.; Kim, S.; Nah, J.; Yang, D.; Piner, R.; Velamakanni, A.; Jung, I.; Tutuc, E.; Banerjee, S. K.; Colombo, L.; Ruoff, R. S. Large-area synthesis of high-quality and uniform graphene films on copper foils. *Science* **2009**, *324*, 1312–4.

(30) Sader, J. E.; Chon, J. W. M.; Mulvaney, P. Calibration of rectangular atomic force microscope cantilevers. *Rev. Sci. Instrum.* **1999**, *70*, 3967–3969.

(31) Li, Q.; Kim, K. S.; Rydberg, A. Lateral force calibration of an atomic force microscope with a diamagnetic levitation spring system. *Rev. Sci. Instrum.* **2006**, *77*, 065105.

(32) Plimpton, S. Fast Parallel Algorithms for Short-Range Molecular-Dynamics. *J. Comput. Phys.* **1995**, *117*, 1–19.

(33) van Duin, A. C. T.; Dasgupta, S.; Lorant, F.; Goddard, W. A. ReaxFF: A reactive force field for hydrocarbons. *J. Phys. Chem. A* **2001**, *105*, 9396–9409.

(34) Rappe, A. K.; Goddard, W. A. Charge Equilibration for Molecular-Dynamics Simulations. *J. Phys. Chem.* **1991**, *95*, 3358–3363.